Project no. GOCE-CT-2003-505539

Project acronym: ENSEMBLES

Project title: ENSEMBLE-based Predictions of Climate Changes and their Impacts

Instrument: Integrated Project

Thematic Priority: Global Change and Ecosystems

Deliverable Reference Number and Title
D.5.26 Model performance in the Indo –Pacific sector (A metric to assess the representation of intraseasonal variability in climate models)

Due date of deliverable: April 2009
Actual submission date: July 2009

Start date of project: 1 September 2004 Duration: 60 Months

Organisation name of lead contractor for this deliverable
Institut Pierre Simon Laplace (IPSL)

Revision [draft, 1, 2, ..]

Project co-funded by the European Commission within the Sixth Framework Programme (2002-2006)		
Dissemination Level		
PU	Public	x
PP	Restricted to other programme participants (including the Commission Services)	
RE	Restricted to a group specified by the consortium (including the Commission Services)	
CO	Confidential, only for members of the Consortium (including the Commission Services)	

An evaluation metric for intraseasonal variability in climate models

PRINCE K. XAVIER * JEAN-PHILIPPE DUVEL

Laboratoire de Meteorologie Dynamique, Ecole Normale Superieure, Paris, France

PASCALE BRACONNOT

Laboratoire des Sciences du Climat et de l'Environnement, Gif-sur-Yvette, France

FRANCISCO J. DOBLAS-REYES

European Centre for Medium-Range Weather Forecasting, Reading, UK

Corresponding author address: Laboratoire de Meteorologie Dynamique, Ecole Normale Superieure, 24 Rue Lhomond, 75231 Paris, France.

E-mail: xavier@lmd.ens.fr

ABSTRACT

The representation of intermittent tropical intraseasonal variability (ISV) in climate models has been conventionally assessed using average statistics which implicitly assume strong reproducibility from one event to the other. A diagnosis on the reproducibility and realism of ISV events is presented here and it is demonstrated that the assumption of strong reproducibility is valid in the observations but not necessarily so in climate models. Based on these diagnostics an objective metric to evaluate the ISV in climate models is presented which measures the resemblance of each simulated large-scale organized ISV event to the most characteristic event in observations. It is applied on the boreal summer ISV over the Indian Ocean in 19 IPCC AR4 models and 7 DEMETER seasonal forecast models. DEMETER version of models produce more reproducible but less realistic ISV patterns compared to the version used in IPCC climate change simulations, due to the initial shock resulting from uncoupled initialization methods used in seasonal forecasts. The Metric bears significant relationship with the redness of the model's rainfall spectra and the accuracy of its summer monsoon rainfall climate. It is implied that correct representation of internal atmospheric processes such as the synoptic weather variability and ISV could reduce the uncertainties in monsoon climate projections.

1. Introduction

The intraseasonal variability (ISV) of the tropical convection is characterized by large scale organized perturbations with maximum amplitudes over the Indo-Pacific region. In boreal winter, they propagate eastward from the western Indian Ocean to the central Pacific and are generally referred to as the Madden-Julian Oscillation, MJO (Madden and Julian 1994). The character of ISV in boreal summer over the Indian Ocean (see Goswami (2005) for a review) is rather distinct. It initiates around 5°S in the eastern Indian Ocean and propagates north-eastward with speed of about 1° latitude per day. With typical periods of 30-40 days, these propagating rain bands reach up to 25°N and contributes largely to the rainfall over India. The summer ISV shows marked seasonality in accordance with the large seasonal variations of Inter Tropical Convergence Zone (ITCZ) over the Indian monsoon region (Bellenger and Duvel 2007). The strong convective ISV center is over the eastern equatorial Indian Ocean in May and redistributes to the Arabian Sea (along the west coast of India) and to the Bay of Bengal in June. The ISV patterns persist for the rest of the monsoon period (July, August and September) but with a reduced amplitude. This seasonality in the ISV is intimately

related to the ocean thermal structure and the atmosphere-ocean feedbacks (Xavier et al. 2008; Bellenger and Duvel 2007; Duvel and Vialard 2007). The ISV is an important component of the Asian summer monsoon system that can modulate the synoptic weather systems (Goswami et al. 2003) and contribute to the seasonal rainfall and its interannual variability (e.g. Goswami et al. 2006). Therefore the accurate representation of the ISV in climate models is important for monsoon forecasting at a range of time scales.

The representation of the ISV in general circulation models (GCMs) has always been a challenge primarily due to its strong dependence on the physical parameterizations (Lin et al. 2008, 2006; Waliser et al. 2003; Sperber et al. 2001; Slingo et al. 1996). In a recent study Xavier et al. (2008) assess the representation of summer ISV over the Indian Ocean in the European climate models participating in the DEMETER (see Section 2) project. Importantly, the lack of large-scale organization of convection was regarded as a major cause of the poor representation of ISV in the DEMETER models. Lin et al. (2008) analyzed the summer ISV represented in 14 IPCC AR4 models (Section 2) and found that the models show a wide range of skill in the representation of summer ISV, often with reduced amplitudes and over-reddened spectrum.

Most of these studies have employed methodologies based either on Empirical Orthogonal Functions (EOFs), correlations, composites or wavenumber-frequency spectral analysis (Wheeler and Weickmann 2001). Xavier et al. (2008) have shown that while the use of an average EOF (or composites) for a season may be robust in the observations, caution should be taken on such a priori assumptions on the robustness of the simulated ISV. As suggested in Goulet and Duvel (2000), for an intermittent phenomenon with large differences between events, the use of a few EOFs or a single composite might result in mathematical objects rather than physical quantities. Lin et al. (2008) present an evaluation of the relative amplitudes of northward wavenumbers (extracted using wave-number frequency spectra between 45°S and 45 °N with constraints on the meridional periodicity). The lead-lag correlations used to compare the northward propagation of rainfall anomalies in the models pertains to the issues mentioned above. An event-wise approach for the assessment of the tropical ISV in the climate models was first introduced by Xavier et al. (2008). This method is based on Local Mode Analysis (LMA) originally developed by Goulet and Duvel (2000). It provides the amplitude, phase, degree of large scale organization and period of each organized convective ISV event. The associated characteristics in other fields such as the sea surface temperature, winds, etc, can also be derived from this analysis.

The objective of this study is to evaluate two major aspects of the intermittent ISV namely i) the reproducibility of the pattern of ISV events and ii) their degree of realism. Based on these diagnostics an evaluation metric is defined which can objectively evaluate the role of different model physics on the representation of ISV. A brief description of the climate models and observations is given in Section 2. The LMA results of summer ISV in IPCC runs and DEMETER hindcasts are described in Section 3. Based on the LMA, measures of the reproducibility and degree of realism of the large-scale organized perturbation patterns of ISV is defined in Section 4 and a model evaluation metric is presented. This metric is applied to evaluate the relationship between high frequency variability and the seasonal mean rainfall climate in the models (Section 5) and results are summarized in Section 6.

2. Models and data

Major international modeling centers have performed long-term simulations of the 20th century climate in order to better assess their representation of the present day climate in preparation to the 21st century climate sensitivity experiments for the IPCC (Intergovernmental Panel on Climate Change) fourth Assessment Report (AR4). Most of the modeling centers used latest versions of their models which incorporates state-of-the-art research results. These include implementation of prognostic cloud microphysics schemes in most models, while some models include trigger on moisture convergence in their deep convection schemes and some take into account convective momentum transport. Moreover, many modeling centers increased their models' horizontal and vertical resolutions and some conducted experiments with different resolutions. Therefore, it is of interest to assess the ISV simulations in this new generation climate models to look at the effects of the updated physical processes, higher resolution, and air-sea coupling. Such an evaluation is also important for evaluating the general performance of the climate models used for climate change projections in the IPCC AR4. The model outputs are archived in the CMIP3 multimodel data base at PCMDI. The details of the horizontal resolution, closure and trigger of different convective schemes in 19 climate IPCC AR4 models are summarized from the IPCC fourth assessment report[1] and are listed in Table 1. Daily rainfall data from the models are used for the computation of ISV. Observed rainfall ISV is derived from the 1 degree-daily (1DD) data of Global Precipitation Climatology Project (GPCP) (Huffman et al. 2001). The rainfall in most models

[1] http://www.ipcc-data.org/ar4/gcm_data.html

cover a period of 40 years, while the 1DD GPCP data is for the period 1997-2006.

A comparison between the performance of IPCC and DEMETER models is also presented. DEMETER is the acronym of the European project entitled 'Development of a European Multi-model Ensemble system for seasonal to inTERannual prediction'. It consists of a suite of 7 coupled European GCMs. For each model uncertainties in the initial conditions are represented through an ensemble of nine different ocean initial conditions. This is achieved by creating three different ocean analyses; a control ocean analysis forced with momentum, heat and mass flux from the ECMWF Reanalysis (ERA40) and two perturbed ocean analyses created by adding small wind stress perturbations. The wind stress perturbations are randomly taken from a set of monthly differences between two quasi-independent analyses. In addition, in order to represent the uncertainties in SSTs, four SST perturbations are added and subtracted at the start of the hindcasts. The atmospheric and land surface initial conditions are taken from the ERA40 data set. A detailed description on the DEMETER models can be found in Palmer et al. (2004). The DEMETER hindcasts starts from 1 February, 1 May, 1 August or 1 November. Each hindcast is an ensemble of nine integrations (nine members) of six months. All seven models have been run for a common period of 1980-2001, although some models have been integrated over an even longer period (1958-2001). In this study, the common period 1980-2001 is used in order to facilitate comparison between models. There are four models (CNRM, INGV, MPI and UKMO) which participated in both DEMETER seasonal forecasting exercise and in the IPCC AR4 runs.

3. Local Mode Analysis of Summer ISV

Spatial patterns and temporal characteristics of the intraseasonal convective events are determined using the LMA (Goulet and Duvel 2000). The LMA makes it possible to detect and characterize in a simple mathematical form the main events of an intermittent phenomenon such as the ISV, that succeed one another in time. It gives a pattern and statistics (amplitude, degree of organization, period, propagation features, etc) for each intraseasonal event and it allows us to compare different events in models and observations. A full description of the approach is given in Goulet and Duvel (2000). Here we give a brief account of the main features of LMA.

The LMA technique is based on a complex EOF (CEOF) computation on a running time section (of 90 days here) on the 20-90 days bandpass filtered precipitation data. For each time step m of the running analysis only the first

CEOF is retained which corresponds to one particular temporal spectrum $\psi^m(k)$ and a spatial perturbation pattern $Z^m(x)$ and explaining a percentage of variance Π^m. k is the temporal harmonic and x is the region. Maxima in the Π^m time series are then identified and the first CEOF of the corresponding time section are called the *Local Modes*. This local mode is assigned with the date of center of the 90-days window. One can demonstrate that the spatial patterns $Z^m(x)$ of these *Local Modes* (or organized convective events) are more persistent in time and more spatially coherent than the CEOF patterns obtained in their neighborhood (Goulet and Duvel 2000).

For a grid point x, the time evolution associated with the local mode of the time step (m) is given by:

$$S^m(x,t) = A^m(x)B^m(t)\cos\left(\phi^m(x) + \chi^m(t)\right) \tag{1}$$

where $A^m(x) = |Z^m(x)|$ and $\phi^m(x) = \arg[Z^m(x)]$ are respectively the regional standard deviation and phase of the leading complex eigenvector $Z^m(x)$. $B^m(t)$ and $\chi^m(t)$ represent respectively the amplitude and phase of the first CEOF of the time section m.

Following the method detailed in Goulet and Duvel (2000), it is possible to compute the average spatial perturbation pattern $\overline{Z}(x)$ from an ensemble of individual intraseasonal events. This is often used to extract the average intraseasonal pattern for a particular month or season (say the summer season; June-September, JJAS). Let they be $\overline{Z}_{obs}(x)$ for the observations and $\overline{Z}_{mod}(x)$ for the models (Fig.1). To have an idea on the number of samples used in this study, GPCP observations has an average of 2.4 organized summer ISV events per year and in the models they range from 2.0 to 2.55 events per year. The average event in the observations ($\overline{Z}_{obs}(x)$,Fig.1a) is based on 24 events (in 10 years). The clockwise rotation of the barbs (representing the phase at a given grid box) indicates the propagation of intraseasonal convection perturbation. In the observations they start at around 85°E, 5°S and propagate northward (with a weak eastward component) to the north Bay of Bengal and the west coast of India. The models show a wide range of skill in reproducing the observed amplitude and propagation characteristics of the average summer ISV ($\overline{Z}_{mod}(x)$, Fig.1). There are a few models (BCCR_b2.0, MPI_ECHAM5) which produce quite realistic average perturbation pattern with their amplitudes and phases resembling the observed pattern. Most models, however, produce either weaker amplitude, shifted convective activity centers or wrong phases of propagation.

4. Reproducibility, realism and model evaluation metric

Unlike in the conventional average diagnostics of ISV, LMA provides more insight into the construction of the average intraseasonal perturbation pattern and its resemblance to the observed. In this study we focus on two important aspects that define the quality of ISV represented in GCMs namely i) the event to event reproducibility of each ISV event and ii) their degree of realism. Since individual intraseasonal events are not necessarily identical, the average spatial perturbation pattern $\overline{Z}(x)$ must be complemented with a measure of its resemblance with the patterns of each event $Z^m(x)$ used to compute it. Such a measure will be useful to verify if the average pattern is representative of the different ISV events, i.e, if it is appropriate to give a physical interpretation of the average pattern or if it is merely a mathematical object resulting from a combination of varied events. This resemblance is computed as the normalized distance $\delta(m)$ between the complex eigenvectors representing the average pattern $\overline{Z}(x)$ and the pattern of each individual event $Z^m(x)$ (Goulet and Duvel 2000). $\delta(m)$ is calculated considering the phase that minimizes the distance between the vectors. Such a minimization is necessary since two eigenvectors that are identical except for a constant phase difference represent actually the same mode. The distance increases as the amplitude and the phase differences between the vectors' components increase. Therefore they compare the spatial distribution of amplitude and phases of each ISV event to the average pattern. The convention is that the patterns are identical for a normalized distance of 0 and orthogonal for a distance of 1. This measure of *reproducibility* in the observations [say $\delta_{rep}(m)$] is computed as the distance between $\overline{Z}_{obs}(x)$ and $Z^m_{obs}(x)$, and for models they are between $\overline{Z}_{mod}(x)$ and $Z^m_{mod}(x)$. The frequency distribution of the distances $\delta_{rep}(m)$ is given in Fig.2. For comparison, the distances of the 7 DEMETER models are also given.

The observed ISV events have all distances less than 0.7 with an median value of 0.36 signifying the robustness of individual ISV events $Z^m_{obs}(x)$ in the construction of the average spatial perturbation pattern [$\overline{Z}_{obs}(x)$]. This justifies the use of average diagnostic such as EOF analysis, composite or regression to describe the Indian Ocean ISV in the observations. But in most models, these distances are quite large (average distance around 0.6 for many models), indicative of rather irregular and less reproducible events. This cautions the use of traditional approaches for ISV evaluation in climate models which a priori assumes ISV being regular and reproducible in the models as in the observations. Such approaches may yield average ISV patterns that are more of mathematical objects constructed by several less-reproducible events in the models and hence a proper physical interpretation of the average perturbation

patterns may be difficult. However, there are some models having reproducibility comparable to the observations (e.g.,BCCR_b2_0, MPI_ECHAM5). The robustness of average patterns presented in Fig.1 depends strongly on these distributions and the average pattern for models with large spread and large average distances must be interpreted with caution, since very few actual intraseasonal perturbation patterns $Z^m_{mod}(x)$ are similar to the average pattern $\overline{Z}_{mod}(x)$. It should, however, be noted that the statistics in this study applies only for the Indian Ocean basin for summer and may vary depending on the size of the basin and the season considered. For instance, Duvel and Vialard (2007) show that these distances are quite small in the observations while considering only the Indian Ocean basin in summer, but larger when considering also the northwest Pacific.

A desirable property of an ISV evaluation metric in GCMs is that it incorporates several elements of model representation of the phenomenon. The approach described above may be extended to evaluate the *degree of realism* of simulated ISV patterns which measures similarity (or difference) in the amplitude, location, phase and, the event to event reproducibility in each model. The distances of individual ISV events in the model, $Z^m_{mod}(x)$ from the average observed summer ISV pattern $\overline{Z}_{obs}(x)$ (Fig.1a) is computed and is called $\delta_{real}(m)$. In the observations $\delta_{real}(m)$ equals $\delta_{rep}(m)$, by definition. The frequency distributions of these distances of the 19 IPCC models along with 7 DEMETER models are given in Fig.3. As expected, these distances are significantly larger for most models compared to those in Fig.2, suggesting that even though some models produce reasonably reproducible ISV events, they are quite far from reality. The average multimodel distance distribution peaks at 0.75. A few models (BCCR_b2_0, MPI_ECHAM5 for instance) produce reasonably reproducible and realistic ISV events.

An objective evaluation metric for the ISV in climate models is derived based on the above diagnostics. The metric[2] is defined for each model as the 50th percentile value (median) of $\delta_{real}(m)$. Therefore, lower the values of the metric, the more realistic the ISV in that model for the particular region and season considered. The metric value is shown as black dots in Fig.3. The models are arranged in the order of their metric value for the Indian Ocean region in boreal summer. As previously mentioned, the values of metric presented here applies to the Indian Ocean region during boreal summer, and they may vary depending on either the region or the season considered. The simulated average intraseasonal perturbation patterns (Fig.1) reveals that the models which have reasonable ISV amplitudes (shades in Fig.1), propagation characteristics (shown as the phases) and locations of convection centers have smaller

[2]A software package to compute the metric is available at http://www.lmd.ens.fr/jpduvel/lma/index_lma.html

values of the metric. The average ISV amplitude decreases for the models with larger values of the metric.

For comparison, the metric for the 7 DEMETER models are also computed and is given in both Fig.2 and 3. There are striking differences when the same version of the model used for IPCC AR4 compared to the DEMETER seasonal hindcasts. Of special mention are MPI ECHAM5, UKMO HadCM3 and the CNRM-CM3 (which is common for CNRM-DMTR, CRFC-DMTR and BCCR B2.0). The reproducibility measure ($\delta_{rep}(m)$) of ISV events to their own average pattern (Fig.2) shows that DEMETER models produce larger number of ISV events which are much more reproducible among themselves than their IPCC AR4 versions. However one can also note the large spread of reproducibility distances ($\delta_{rep}(m)$) in DEMETER compared to the IPCC version. They also tend to produce much less realistic events as revealed by the larger realism distances $\delta_{real}(m)$ (Fig.3).

The DEMETER system uses separate atmosphere and ocean initial states (Section 2) generated acknowledging the errors in the uncoupled component models, but they are constructed without recognition of the errors in the coupled model. In reality, the sub-surface ocean thermal state associated with ocean initial conditions is significantly different from the climate of the free running coupled model as in the IPCC runs. As a consequence, at forecast initialization, the coupled model can rapidly adjust away from the observed climate estimates towards the coupled model climate. This adjustment is primarily accomplished via equatorial waves (Moore 1989), which ultimately lead to an erroneous SST response 2-4 months into the forecast evolution. This SST adjustment towards model climate could possibly introduce some unrealistic, but rather reproducible model errors that LMA could detect as ISV patterns in the initial months of the seasonal forecasts. This may explain the larger reproducibility of ISV patterns (Fig.2) and poor realism (Fig.3) in DEMETER compared to IPCC runs by the same model. The improved representation of ISV in BCCR B2.0 over that of CNRM-CM3 may also be due to the fact that sea surface current is accounted for the turbulent surface fluxes computation (Frode Flatoy, personal communication). However, the exact nature and causes of these differences would require specific studies using these models.

The ability of a model to simulate the large-scale organization of the ISV of the convection may also be diagnosed using LMA results. This diagnostic is based on the regional LMA variance $A^m(x)^2$ of each event. This LMA variance is the part of the signal having common spectral characteristics with other regions (the spectral key $\psi^m(k)$) during the intraseasonal event. The ratio between the LMA variance and the variance of the 20-90 day signal over the same time segment is thus an indicator of the part of the local signal corresponding to the large-scale intraseasonal

perturbation. The average ratio over all intraseasonal events (Fig.4) thus highlights regions strongly impacted by large-scale organized events. The observed ratio is the largest (with values larger than 0.7) over the eastern equatorial Indian Ocean, which is a source region of the convective intraseasonal perturbations in summer. The high values over Bay of Bengal and Eastern Arabian Sea suggest that most of the ISV of the convection over this region is due to large-scale organized convective perturbations. The ratio for each model is arranged according the metric in Fig.3. For models with a good ISV metric, the ratio is comparable to the observations in both magnitude and location, with in particular a maximum ratio for the east equatorial Indian Ocean. Models with a poor ISV metric tend to produce smaller ratio and, generally, wrong position of the maximum values. A smaller ratio reveals that large-scale organized events have a weaker impact on the regional ISV. A possible consequence is that the convective heating perturbation is organized at a smaller scale, giving a too weak dynamical response. The link between the ratio and the ISV metric thus suggest that part of the problem in simulating the ISV can be related to the lack of large-scale organization of the convection, either for the triggering of the ISV events or for its evolution.

5. Scale interactions

Kitoh (2006) presents a review on the future changes of the South Asian summer monsoon due to CO2 increase as projected by the state-of-the-art climate models. Although a few studies reported that the South Asian summer monsoon becomes weak or there is no significant change in precipitation (Zhao and Kellogg 1988; Lal and Singh 2001), most models show that the seasonal mean precipitation increases and interannual variability increases as well (Meehl and Washington 1993; Bhaskaran et al. 1995; Kitoh et al. 1997; Douville et al. 2000; Meehl and Arblaster 2003). The projections of these regional-scale climate changes, however, are highly model-dependent and there are large differences among models for projected changes in monsoon precipitation, including even the sign of change [Kitoh (2006) and references therein]. The seamless prediction paradigm (Palmer et al. 2008) postulates that the large uncertainties in the projected climate change are at least due in part to the fact that the models do not accurately capture the weather-climate link. ISV is known as an important component of the monsoon system that interacts with the synoptic weather events and the seasonal mean and interannual variations (Goswami et al. 2006). How accurate the statistics of the collection of synoptic weather systems at the high frequency (HF) end of the spectrum is represented

in a model can possibly influence the ISV and seasonal to interannual time scales and beyond. The ISV evaluation metric defined in this study can be a useful tool in assessing the link between the high-frequency variability and the climatology of IPCC models. In this section we examine the relationship between the HF variability, the ISV representation and the monsoon precipitation climatology in each model and observations.

The Fourier power spectra of the detrended time series of precipitation for each grid point in the domain 70°-100°E, Eq-25°N for each summer is calculated and the average spectra is shown in Fig.5a. Most models have HF power seriously underestimated, and only a couple of models produce realistic variance in the 10-60 days band. Intriguingly, contrary to the observations, all models produce strongly reddened power spectra (with large power at low frequencies) as noted by Lin et al. (2008) as well. The redness of the spectrum of each model is estimated by the ratio between variances in the intraseasonal and the HF band. A comparison of the ratio and the model evaluation metric (Fig.5b) shows a significant (r = 0.58 at 99 % level) relationship. Models that tend to produce realistic intraseasonal perturbation patterns have more realistic variance (Fig.5c) and have reduced and more realistic spectral redness.

The simulated seasonal average rainfall distribution can be evaluated by computing the spatial correlation between simulated and observed rainfall maps. Since the ISV modulates the position of the ITCZ in the course of the monsoon season, there may be a link between the characteristics of the ISV events and the average rainfall distribution. One could therefore try to verify if models with a good ISV metric also produce a good average rainfall distribution. A correlation of -0.76 (significant at 99% level) suggests a strong tendency for models with better ISV realism metric to have more spatially consistent monsoon rainfall climatology (Fig.6). It is however not trivial to establish a direction of causality for such a link since a correct location of the convective variability at all time scales (synoptic to intraseasonal) is obviously dependent on the correct location of the ITCZ. The ISV realism metric takes implicitly this fact into account since a small distance between observed and simulated ISV patterns request a correct simulation of the main rainfall areas. In such a case, the ISV realism metric will be mathematically related to this correlation and hide a possible effect of the ISV on the representation of the average rainfall distribution. However, the ISV reproducibility (Fig.2) is independent of the observed average rainfall distribution and can be compared. A link between these two factors will indicate that the ability of a model to give reproducible ISV events is somewhat linked to its ability to give a correct average rainfall distribution. There is indeed a correlation of -0.44 between these two factors that is significant at 95% level. This may also indicate that well organized and reproducible ISV events can develop only in

realistic mean states. The precise knowledge of the origin of this link needs analyses that are outside the scope of this study.

6. Summary and discussions

Diagnostics on the representation of summer ISV over the Indian Ocean in the IPCC models is presented with focus on its event to event reproducibility and realism. The LMA used here provides a measure of the reproducibility and realism by identifying in a single mathematical form, the perturbation pattern of each individual organized convective ISV event. This measure evaluates the robustness of the average ISV perturbation pattern (Fig.1). Secondly, the resemblance of simulated ISV events to a typical observed pattern is measured for each simulated ISV event and the most probable distance is presented as a metric for evaluating the simulation of tropical ISV. This gives an objective evaluation of simulated ISV in terms of their amplitude, propagation characteristics and reproducibility from one event to the other.

The models show a wide range of skills in representing the ISV. There are a few models which produce realistic amplitude, propagation characteristics and event to event reproducibility. Xavier et al. (2008) focused the analysis on the air-sea interactions and pointed out few issues in representing the intraseasonal air-sea interaction processes. The lack of representation of diurnal SST variability and the associated coupled feedbacks were proposed to be a source of the DEMETER model biases. This, however, would require experiments with models that can resolve the oceanic mixed layer and exchange of fluxes with the atmosphere at sub-diurnal intervals. The convective parameterization is known to have a strong impact in the climate models whose signatures can be found even in the deep ocean circulation (Braconnot et al. 2007). In the AMIP I simulations, Slingo et al. (1996) noted that the models with reasonable level of intraseasonal activity used convection schemes that were closed on buoyancy rather than moisture supply. Several recent analysis demonstrated improved MJO simulations for models with mass-flux convection schemes that use adjustment type of closures (Liu et al. (2005). However these findings may be arguable since Wang and Schlesinger (1999) demonstrated that it is possible to alter substantially the strength of MJO by modifying the particular trigger used within the convection scheme as well as the fundamental scheme itself. The large sensitivity of ISV simulation demands more dedicated analysis before any conclusions are drawn on the advantages or drawbacks of any particular

convection scheme. Considering that the large-scale convective organization depends largely on the convective parameterization, our metric is able to classify the models based on the convective organization and thereby highlights the need for improvements in convection schemes. This enhances the utility of the metric as a diagnostic tool since it can evaluate the drawbacks in parameterized physics and the complex feedbacks.

The use of a model in initialized seasonal forecasting mode (as in DEMETER) and as a free running coupled model (as in IPCC AR4) brings out a few interesting points. The DEMETER version often produces more reproducible, but less realistic ISV patterns compared to the IPCC version. The capacity of a initialized forecast to represent ISV in the initial few months could be seriously affected by the possible errors due to the initialization shock and its subsequent adjustment in the ocean towards model climate. The exact behavior of these errors and their adjustment requires detailed analysis. Another observations is that, as shown in the Table 1, the BCCR and CNRM models have the same atmospheric model (ARPEGE-CLIMAT Version 3) and there is a marked improvement in the ISV amplitude in BCCR compared to CNRM, even though the spatial structure of ISV remains nearly the same. This improvement could be attributed to a modification in which the sea surface current is accounted for when the turbulent surface fluxes are computed. The extent to which surface fluxes are affected by this modification is not known, but it certainly signifies the importance for accurate modeling of atmosphere-ocean fluxes to represent realistic ISV properties.

The ISV evaluation metric bears significant relationship with the representation of both day-to-day variance and seasonal mean climate. In a seamless modeling context, it is postulated that synoptic scale weather systems could possibly impact the ISV through the modification of ocean heat content and the associated air-sea interaction processes. An important link that bridge the gap between weather and climate over the Asian monsoon region is the ISV and its realistic representation is certainly important to produce a reasonable mean state. The issue is thus to know what are the important missing elements for a correct representation of the internal variability and what is the best strategy for incorporating them into the coupled models. Interestingly, most models producing reddened rainfall spectra also produce a too weak day-to-day variance. As suggested by Lin et al. (2008), the weak day-to-day variance could result from the absence of self-suppression mechanisms of convection in the models. For example, the dry (or unsaturated) downdrafts associated with the convection can cool the surface, reduce the temperature and humidity gradients at the lower troposphere, thereby reducing the buoyancy and moisture availability at the surface. Such a mechanism has the potential to suppress the convective activity for the days following organized active convective spell. This gives thus

a larger day-to-day variance of the precipitation at both synoptic and intraseasonal time-scales. By contrast, models with poor day-to-day variability will exhibit mostly a slow evolution of the precipitation field, following more the seasonal forcing and resulting in an over-reddened spectrum. This 'reddish' character will be reduced for model with a better day-to-day variance, explaining why these models also have a more realistic spectrum. According to our metrics, these are also models with the better ISV in the tropics, showing the potential importance of the mechanisms described above.

Acknowledgments.

The IPCC AR4 data is obtained from the WCRP CMIP3 multi-model database. We thank the Program for Climate Model Diagnosis and Intercomparison (PCMDI) for collecting and archiving the CMIP3 model output, and the WCRP Working Group on Coupled Modeling (WGCM) for organizing the model data analysis activity. GPCP 1DD data is obtained from *http://www1.ncdc.noaa.gov/pub/data/gpcp/1dd/data/*. Authors thanks Hervé Douville for his comments on a previous version of the article. PKX and FJDR are supported by the European ENSEMBLES project.

REFERENCES

Bellenger, H. and J. P. Duvel, 2007: Intraseasonal convective perturbations related to the seasonal march of the Indo-Pacific monsoons. *J. Climate*, **20**, 2853–2863.

Betts, A. K., 1986: A new convective adjustment scheme. Part I. .Observational and theoretical basis. *Quart. J. Roy. Meteor. Soc.*, **112**, 677–691.

Bhaskaran, B., J. Mitchell, J. Lavery, and M. Lal, 1995: Climatic response of the Indian subcontinent to doubled CO2 concentrations. *Int. J. Climatol.*, **15**, 873–892.

Bougeault, P., 1985: A simple parameterization of the large-scale effects of cumulus convection. *Mon. Wea. Rev.*, **113**, 2108–2121.

Braconnot, P., F. Hourdin, S. Bony, J. L. Dufresne, J. Y. Grandpeix, and O. Marti, 2007: Impact of different convective cloud schemes on the simulation of the tropical seasonal cycle in a coupled oceanatmosphere model. *Climate Dyn.*, **29**, 501–520.

Douville, H., J.-F. Royer, J. Polcher, P. Cox, N. Gedney, D. Stephenson, and P. Valdes, 2000: Impact of CO2 doubling on the Asian summer monsoon: Robust versus model-dependent responses. *J. Meteor. Soc. Japan*, **78**, 421–439.

Duvel, J. P. and J. Vialard, 2007: Indo-Pacific sea surface temperature perturbations associated with intraseasonal oscillation of the tropical convection. *J. Climate*, **20**, 3056–3082.

Emanuel, K. A., 1991: A scheme for representing cumulus convection in large-scale models. *J. Atmos. Sci.*, **48**, 2313–2335.

Goswami, B., G. Wu, and T. Yasunari, 2006: Annual cycle, intraseasonal oscillations and roadblock to seasonal predictability of the asian summer monsoon. *J. Climate*, **19**, 5078–5099.

Goswami, B. N., 2005: The Asian Monsoon: Interdecadal variability. *The Global Monsoon System: Research and Forecast*, N.-C. G. L. C.-P. Chang, Bin Wang, Ed., WORLD METEOROLOGICAL ORGANIZATION, WMO/TD No. 1266, 455.

Goswami, B. N., R. S. Ajayamohan, P. K. Xavier, and D. Sengupta, 2003: Clustering of low pressure systems during the Indian summer monsoon by intraseasonal oscillations. *Geophys. Res. Lett.*, **30(8) (1431)**, doi:10.1029/2002GL016 734.

Goulet, L. and J. P. Duvel, 2000: A new approach to detect and characterize intermittent atmospheric oscillations: Application to the intraseasonal oscillation. *J. Atmos. Sci.*, **57**, 2397–2416.

Gregory, D. and P. R. Rowntree, 1990: A mass flux convection scheme with representation of cloud ensemble characteristics and and stability dependent closure. *Mon. Wea. Rev.*, **118**, 1483–1506.

Huffman, G. J., R. Adler, M. Morrissey, D. Bolvin, S. Curtis, R. Joyce, B. McGavock, and J. Susskind, 2001: Global precipitation at one-degree daily resolution from multi-satellite observations. *J. Hydrometeor.*, **2**, 36–50.

Kitoh, A., 2006: Asian monsoons in future. *The Asian Monsoon*, B. Wang, Ed., Springer/Praxis Publishing, New York, 631–649.

Kitoh, A., S. Yukimoto, A. Noda, and T. Motoi, 1997: Simulated changes in the Asian summer monsoon at times of increased atmospheric CO2. *J. Meteor. Soc. Japan*, **75**, 1019–1031.

Lal, M. and S. K. Singh, 2001: Global warming and monsoon climate. *Mausam*, **52**, 245–262.

Lin, J. L., K. Weickman, G. Kiladis, B. Mapes, S. Schubert, M. Suarez, J. Bacmeister, and M. Lee, 2008: Subseasonal variability associated with Asian summer monsoon simulated by 14 IPCC AR4 Coupled GCMs. *J. Climate*, **21**, 4541–4567.

Lin, J. L., et al., 2006: Tropical intraseasonal variability in 14 IPCC AR4 climate models. Part I: Convective signals. *J. Climate*, **19 (12)**, 2665–2690.

Liu, P., B. Wang, K. Sperber, T. Li, and G. Meehl, 2005: MJO in the NCAR CAM2 with the Tiedtke convective scheme. *J. Climate*, **18**, 3007–3020.

Madden, R. A. and P. R. Julian, 1994: Observations of the 40-50 day tropical oscillation: A review. *Mon. Wea. Rev.*, **122**, 813–837.

Meehl, G. A. and J. Arblaster, 2003: Mechanisms for projected future changes in south Asian monsoon precipitation. *Clim. Dyn.*, **21**, 695–675.

Meehl, G. A. and W. M. Washington, 1993: South Asian summer monsoon variability in a model with doubled atmospheric carbon dioxide concentration. *Science*, **260**, 1101–1104.

Moore, A. M., 1989: Aspects of geostrophic adjustment during tropical ocean data assimilation. *J. Phys. Oceanogr.*, **19**, 435–461.

Moorthi, S. and M. J. Suarez, 1992: Relaxed Arakawa-Schubert: A parameterization of moist convection for general circulation models. *Mon. Wea. Rev.*, **120**, 978–1002.

Nordeng, T. E., 1994: *Extended versions of the convective parameterization scheme at ECMWF and their impact on the mean and transient activity of the model in the tropics*. Reading, UK, European Centre for Medium-Range Weather Forecasting, ECMWF Technical Memorandum 206.

Palmer, T. N., F. Doblas-Reyes, A. Weisheimer, and M. Rodwell, 2008: Toward seamless prediction: Calibration of climate change projections using seasonal forecasts. *Bull. Amer. Meteor. Soc.*, **89**, 459–470.

Palmer, T. N., et al., 2004: Development of a European multimodel ensemble system for seasonal-to-interannual prediction (DEMETER). *Bull. Amer. Meteor. Soc.*, DOI: 10.1175/BAMS–85–6–853.

Pan, D.-M. and D. A. Randall, 1998: A cumulus parameterization with a prognostic closure. *Quart. J. Roy. Meteor. Soc.*, **124**, 949–981.

Russell, G. L., M. J. R., and D. Rind, 1995: A coupled atmosphere-ocean model for transient climate change studies. *Atmos-Ocean*, **33**, 683–730.

Slingo, J. M., et al., 1996: Intraseasonal oscillations in 15 atmospheric general circulation models: Results from an AMIP diagnostic subproject. *Climate Dyn.*, **12**, 325–357.

Sperber, K. R., et al., 2001: Dynamical seasonal predictability of the Asian summer monsoon. *Mon. Wea. Rev.*, **129**, 2226–2248.

Tiedtke, M., 1989: A comprehensive mass flux scheme for cumulus parameterization in large-scale models. *Mon. Wea. Rev.*, **117**, 1779–1800.

Waliser, D. E., et al., 2003: AGCM simulations of intraseasonal variability associated with the Asian summer monsoon. *Climate Dyn.*, **21**, 423–446.

Wang, W. and M. E. Schlesinger, 1999: The dependence on convection parameterization of the tropical intraseasonal oscillation simulated by the UIUC 11-layer atmospheric GCM. *J. Climate*, **12**, 1423–1457.

Wheeler, M. and K. Weickmann, 2001: Realtime monitoring and prediction of modes of coherent synoptic to intraseasonal tropical variability. *Mon. Wea. Rev.*, **129**, 2677–2694.

Xavier, P. K., J.-P. Duvel, and F. J. Doblas-Reyes, 2008: Boreal summer intraseasonal variability in coupled seasonal hindcasts. *J. Climate*, **21**, 4477–4497.

Zhang, G. J. and N. A. McFarlane, 1995: Sensitivity of climate simulations to the parameterization of cumulus convection in the Canadian Climate Centre General Circulation Model. *Atmos.-Ocean*, **33**, 407–446.

Zhao, Z. and W. Kellogg, 1988: Sensitivity of soil moisture to doubling of carbon dioxide in climate model experiments. Part II: The Asian monsoon region. *J. Climate*, **1**, 367–378.

List of Tables

1 IPCC AR4 models and their AGCM features 19

TABLE 1. IPCC AR4 models and their AGCM features

Model label	Institution	Equivalent Grid resolution	Deep Convection
bccr_b2_0	Bjerknes Centre for Climate Research, Norway	2.8×2.8°(T42)	Bougeault (1985)
mpi_echm5	Max Planck Inst. for Meteorology, Germany	2.8×2.8°(T42)	Tiedtke (1989) Nordeng (1994)
echo_miug	Meteorological Inst. Univ. of Bonn, Germany	3.75×2.8°(T30)	Tiedtke (1989)
cnrm_cm_3	Centre National de Recherches Météorologiques, France	2.8×2.8°(T42)	Bougeault (1985)
gfdl_c2_0	NOAA/GFDL, USA	2.5×2.0°	Moorthi and Suarez (1992)
csiro_3_0	CSIRO, Australia	1.875×1.875°(T63)	Gregory and Rowntree (1990)
ukmo_hcm3	UK Met Office	1.25×1.875°	Gregory and Rowntree (1990)
mri_2_3_2	Meteorological Research Institute, Japan	2.8×2.8°(T42)	Pan and Randall (1998)
miro_mres	Center for Climate System Research,Japan	2.8×2.8°(T42)	Pan and Randall (1998)
csiro_3_5	CSIRO, Australia	1.875×1.875°(T63)	Gregory and Rowntree (1990)
ingv_ech4	Istituto Nazionale di Geofisica e Vulcanologia, Italy	3.75×2.8°(T30)	Tiedtke (1989)
ncar_csm3	NCAR, USA	1.4×1.4°(T85)	Zhang and McFarlane (1995)
ncar_pcm1	NCAR, USA	2.8×2.8°(T42)	Zhang and McFarlane (1995)
cgcm3_T47	Canadian Centre for Climate Modeling and Analysis, Canada	2.5×2.5°(T47)	Zhang and McFarlane (1995)
cgcm3_T63	Canadian Centre for Climate Modeling and Analysis, Canada	1.875×1.875°(T63)	Zhang and McFarlane (1995)
ipsl_cm_4	Institut Pierre Simon Laplace, France	3.75×2.5°	Emanuel (1991)
inm_cm3_0	Institute of Numerical Mathematics, Russia	5×4°	Betts (1986)
fgoals1_0	Chinese Academy of Sciences China	5×4°	Zhang and McFarlane (1995)
giss_aom1	NASA/GISS, USA	4×3°	Russell et al. (1995)

List of Figures

1 The average patterns of precipitation ISV for the summer (JJAS) from the observations and the IPCC models. Shades represent the standard deviation of the ISV in mm day^{-1}. The segment represents the phase of the propagation and its length is proportional to the standard deviation. The angle of segment (phase) increases clockwise with time (e.g. northward propagation for a segment rotating clockwise towards the north). The number of local modes used to construct each pattern is indicated on the top left of each panel. For example, the observed pattern is constructed from 24 events in the 10 years, while in the models it is constructed from a larger number of events. 22

2 Distribution of distances between individual ISV events to their average summer ISV pattern in the observations and models. The bars range from the 25th percentile to the 75th percentile value. The horizontal line represents the range of values and the median (50th percentile) values are represented by the vertical lines on each bar. 23

3 Distribution of distances between individual ISV events to the observed average summer ISV pattern in the observations and models.The bars range from the 25th percentile to the 75th percentile value. The line represents the range of values. The median (50th percentile) values are denoted by the black dots. Models are arranged according to the median distance. 24

4 Ratio of amplitude of each individual large scale organized ISV event over a 90 days time segment to the amplitude of the 20-90 days bandpass filtered rainfall amplitude over the same time segment. The value for a particular region represents the average contribution of large-scale organized convective perturbations to the local, more stochastic (or related to local instability) rainfall variability. 25

5 (a) Detrended power spectra of JJAS rainfall averaged over 70°- 100°E, Eq-25°N in the observations and the models. (b) shows the relationship of the ISV metric to the redness of the spectra defined as the ratio of 10-60 days variance to the 2-10 days variance. The relationship between the metric and total variance in the 2-60 days band is shown in (c). Each model is marked with a number as in Fig.3 according to the metric. The linear correlation values in (b) and (c) are indicated. 26

6 The relationship between the ISV metric and the spatial correlation between simulated and observed climatological rainfall over 60°-110°E, 20°S-25°E. Each model is marked with a number as in Fig.3 according to the metric. The linear correlation value is -0.76. 27

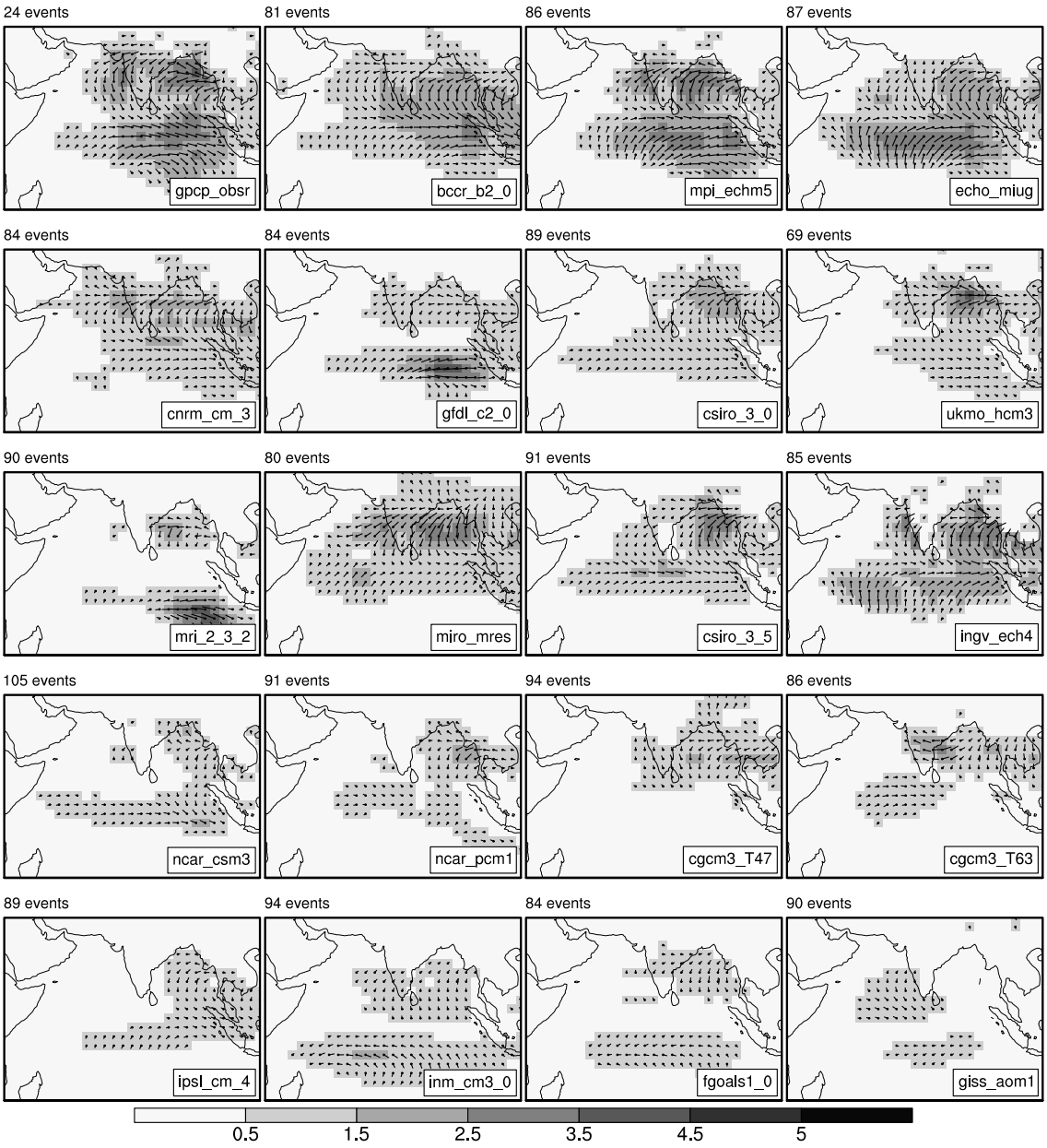

FIG. 1. The average patterns of precipitation ISV for the summer (JJAS) from the observations and the IPCC models. Shades represent the standard deviation of the ISV in mm day^{-1}. The segment represents the phase of the propagation and its length is proportional to the standard deviation. The angle of segment (phase) increases clockwise with time (e.g. northward propagation for a segment rotating clockwise towards the north). The number of local modes used to construct each pattern is indicated on the top left of each panel. For example, the observed pattern is constructed from 24 events in the 10 years, while in the models it is constructed from a larger number of events.

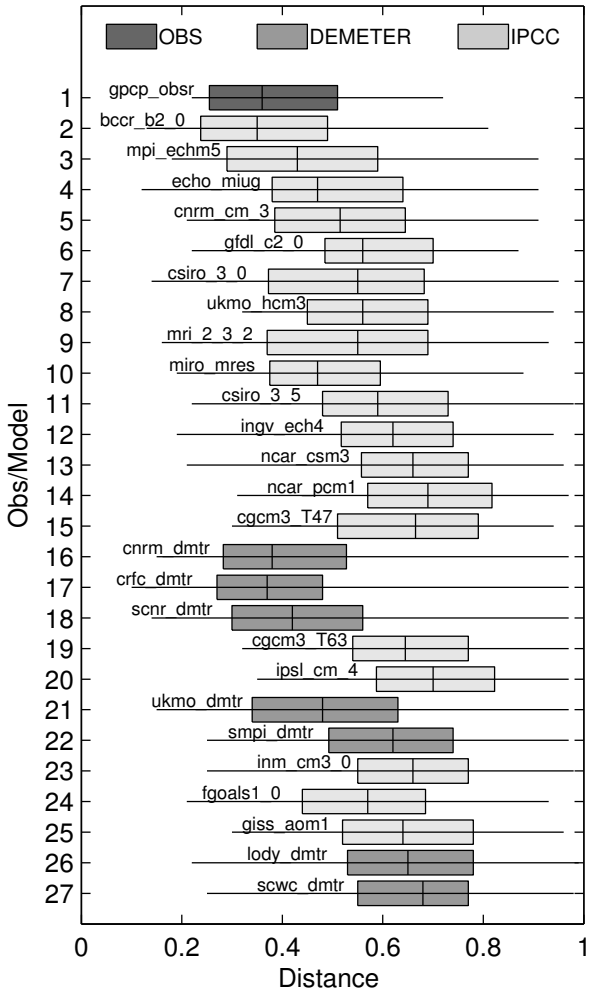

FIG. 2. Distribution of distances between individual ISV events to their average summer ISV pattern in the observations and models. The bars range from the 25th percentile to the 75th percentile value. The horizontal line represents the range of values and the median (50th percentile) values are represented by the vertical lines on each bar.

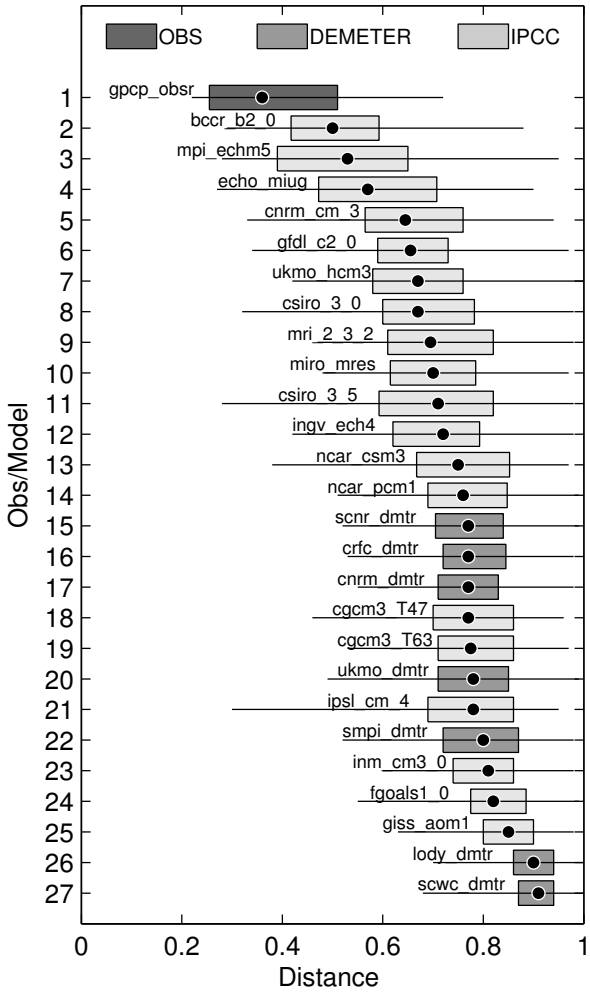

FIG. 3. Distribution of distances between individual ISV events to the observed average summer ISV pattern in the observations and models.The bars range from the 25th percentile to the 75th percentile value. The line represents the range of values. The median (50th percentile) values are denoted by the black dots. Models are arranged according to the median distance.

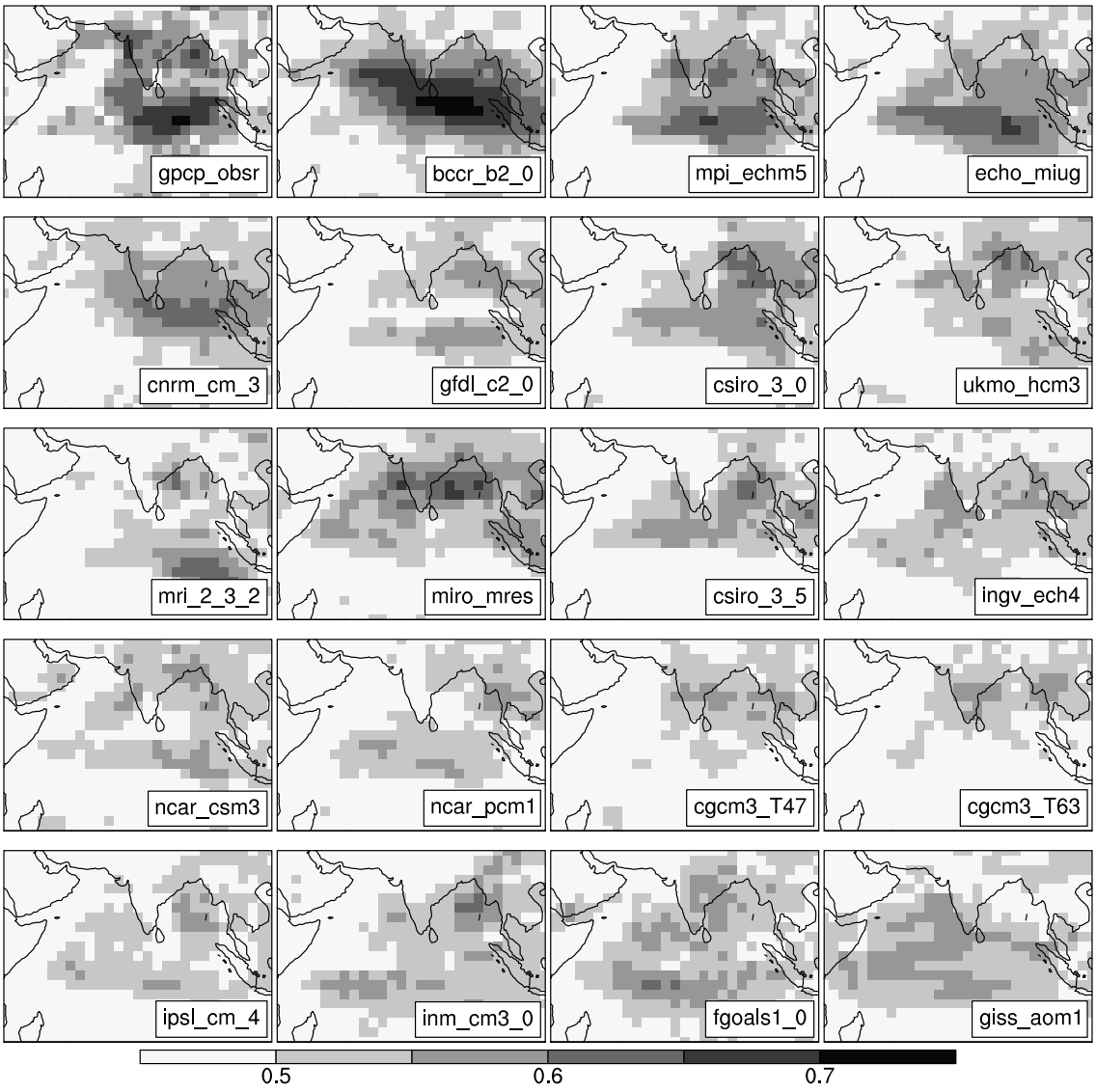

FIG. 4. Ratio of amplitude of each individual large scale organized ISV event over a 90 days time segment to the amplitude of the 20-90 days bandpass filtered rainfall amplitude over the same time segment. The value for a particular region represents the average contribution of large-scale organized convective perturbations to the local, more stochastic (or related to local instability) rainfall variability.

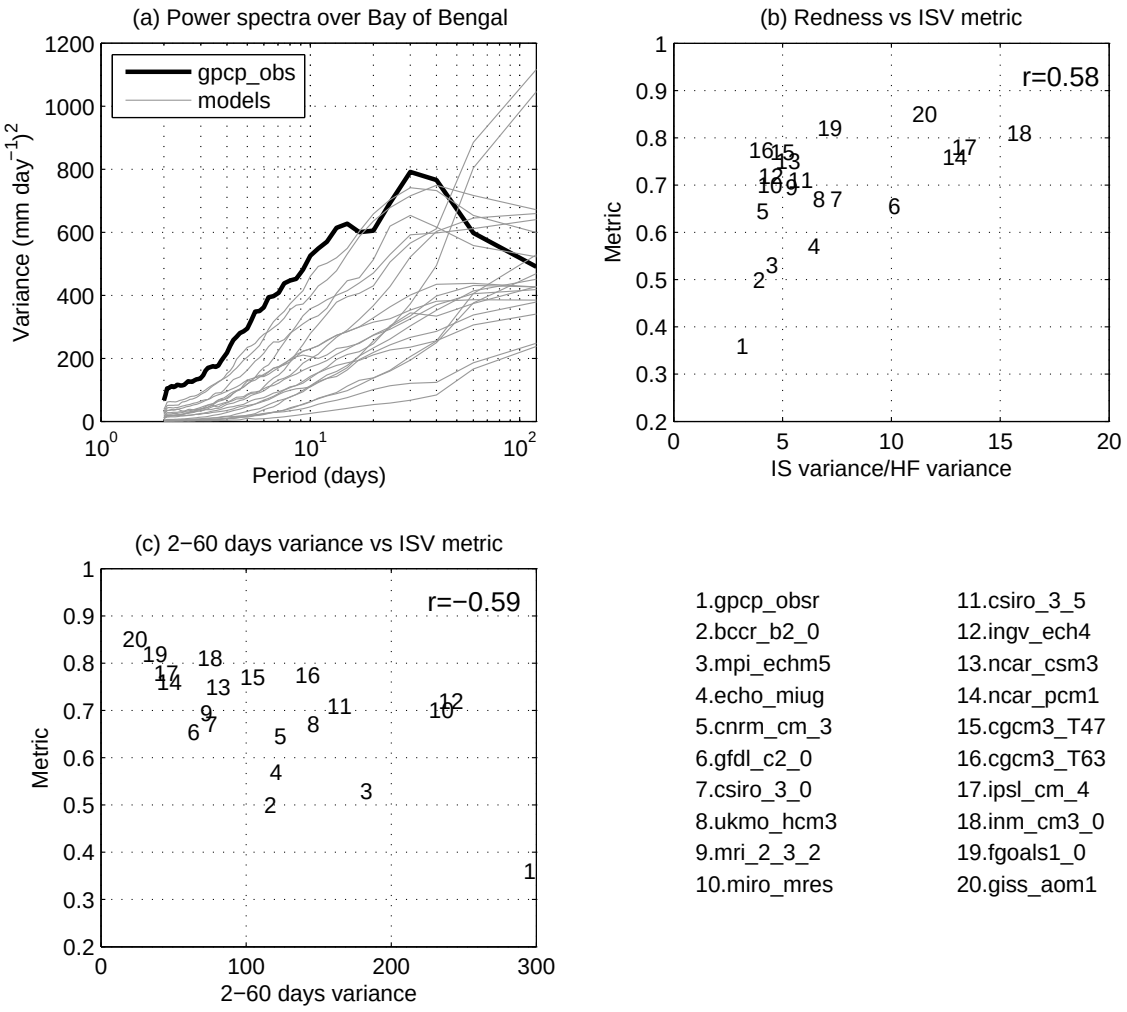

FIG. 5. (a) Detrended power spectra of JJAS rainfall averaged over 70°- 100°E, Eq-25°N in the observations and the models. (b) shows the relationship of the ISV metric to the redness of the spectra defined as the ratio of 10-60 days variance to the 2-10 days variance. The relationship between the metric and total variance in the 2-60 days band is shown in (c). Each model is marked with a number as in Fig.3 according to the metric. The linear correlation values in (b) and (c) are indicated.

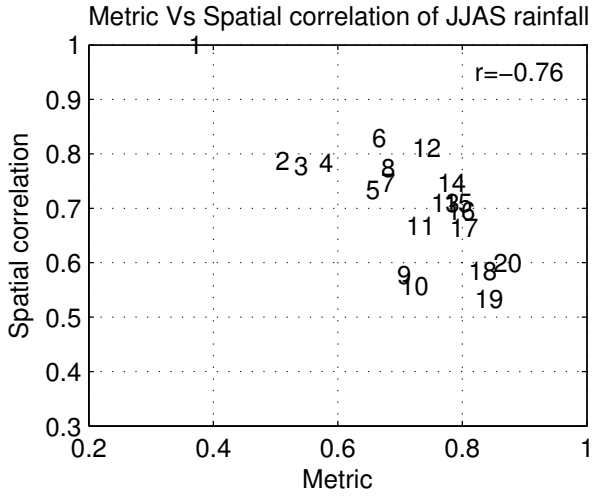

FIG. 6. The relationship between the ISV metric and the spatial correlation between simulated and observed climatological rainfall over 60°-110°E, 20°S-25°E. Each model is marked with a number as in Fig.3 according to the metric. The linear correlation value is -0.76.